12:01:36 • OCA PAD AMENDMENT - PROJECT HEADER INFORMATION 12/05/92

Active

Project #: E-19-655 Cost share #: Rev #: 1
Center # : 10/24-6-R7241-0A0 Center shr #: OCA file #:
Work type : RES
Contract#: RI-B-91-18 Mod #: LTR OF 921130 Document : GRANT
Prime #: Contract entity: GTRC

Subprojects ? : N CFDA: N/A
Main project #: PE #: N/A

Project unit: CHEM ENGR Unit code: 02.010.114
Project director(s):
KOHL P CHEM ENGR (404)894-2893

Sponsor/division names: AMER INST CHEMICAL ENGRS /
Sponsor/division codes: 500 / 022

Award period: 910901 to 930401 (performance) 930401 (reports)

Sponsor amount	New this change	Total to date
Contract value	0.00	23,000.00
Funded	0.00	23,000.00
Cost sharing amount		0.00

Does subcontracting plan apply ?: N

Title: LOW TEMPERATURE CVD REACTOR FOR SILICON PASSIVATION

PROJECT ADMINISTRATION DATA

OCA contact: Kathleen R. Ehlinger 894-4820

Sponsor technical contact	Sponsor issuing office
DR. CHARLES V. FREIMAN (212)705-7835	DR. CHARLES V. FREIMAN (212)705-7835
ENGINEERING FOUNDATION 345 EAST 47TH STREET NEW YORK, NY 10017	ENGINEERING FOUNDATION 345 EAST 47TH STREET NEW YORK, NY 10017

Security class (U,C,S,TS) : U ONR resident rep. is ACO (Y/N): N
Defense priority rating : N/A N/A supplemental sheet
Equipment title vests with: Sponsor X GIT
NONE PROPOSED.
Administrative comments -
ISSUED TO EXTEND TERMINATION DATE FROM 8/31/92 TO 4/1/93.

GEORGIA INSTITUTE OF TECHNOLOGY
OFFICE OF CONTRACT ADMINISTRATION

NOTICE OF PROJECT CLOSEOUT

Closeout Notice Date 12/23/92

Project No. E-19-655 Center No. 10/24-6-R7241-0A0

Project Director KOHL P School/Lab CHEM ENGR

Sponsor AMER INST CHEMICAL ENGRS/

Contract/Grant No. RI-B-91-18 Contract Entity GTRC

Prime Contract No.

Title LOW TEMPERATURE CVD REACTOR FOR SILICON PASSIVATION

Effective Completion Date 930401 (Performance) 930401 (Reports)

Closeout Actions Required:	Y/N	Date Submitted
Final Invoice or Copy of Final Invoice	Y	
Final Report of Inventions and/or Subcontracts	N	
Government Property Inventory & Related Certificate	N	
Classified Material Certificate	N	
Release and Assignment	N	
Other	N	

Comments EFFECTIVE DATE 9-1-91. CONTRACT VALUE $23,000.

Subproject Under Main Project No.

Continues Project No.

Distribution Required:

Project Director	Y
Administrative Network Representative	Y
GTRI Accounting/Grants and Contracts	Y
Procurement/Supply Services	Y
Research Property Managment	Y
Research Security Services	N
Reports Coordinator (OCA)	Y
GTRC	Y
Project File	Y
Other HARRY VANN-FMD	Y
FRED CAIN-OOD	Y

E-19-655

LOW TEMPERATURE CVD REACTOR FOR SEMICONDUCTOR PASSIVATION

Interim Report
Contract # RI-B-91-18
March 1, 1992

Kirkland W. Vogt and Paul A. Kohl
Georgia Institute of Technology
Atlanta, GA 30332-0100
404-894-2893

INTRODUCTION

The objective of this work is to investigate the fundamental chemical engineering concepts in producing low temperature metal nitride films. The primary application of these nitrides is the passivation of III-V compound semiconductors. Other areas of importance are the stabilization of transition metals such as titanium and iron, and the passivation of silicon.

Commonly, nitride films are created using plasma-enhanced or high temperature decomposition of ammonia (i.e. 800^0-1000^0C). Unfortunately, these conditions are not always desirable because crystalline defects and the decomposition of metal and semiconductor substrates can occur. Also, secondary reactions with oxygen and water can produce undesirable oxides. Many oxides react further with the III-V semiconductor to produce conductive layers at the oxide-semiconductor interface. Several researchers have concluded that the presence of oxygen in any III-V semiconductor passivation process will create device failure problems for integrated circuits.(1)

REACTOR SPECIFICATIONS:

A reactor and reaction sequence have been designed to eliminate high temperatures, high-energy particles, and oxygen and water impurities. Ideally, the design should:

(1) produce nitride surfaces for III-V semiconductors and transition metals,

(2) have a deposition temperature below the decomposition temperature of III-V semiconductors and the other materials present,

(3) not use plasma-enhanced reactions,

(4) contain cleaning reactions for the removal of any native oxides and atmospheric contaminants,

(5) provide very low oxygen and water concentrations to minimize competing reactions,

(6) produce a chemically stable material that provides protection from water and oxygen, and

(7) generate a hard, thick, protective film.

The following reaction sequence is being investigated.

1. Removal of undesirable oxides: A conventional clean/etch is used to remove any thick oxides and carbon deposits.[2] After the clean/etch, the III-V semiconductor is introduced into the reactor. Next, the oxides are removed with hydrogen (H_2) or hydrogen chloride (HCl) and H_2 at 200^{0}C to 400^{0}C. Several other researchers have investigated in-situ oxide removal with H_2 or HCl. Barbouth, et al, [3] heated gallium arsenide (GaAs) at 550^{0}C and indium phosphide (InP) at 350^{0}C in H_2 to remove oxides from the surface. Saito, et al [4-6] has had success cleaning GaAs with HCl and H_2. They obtained atomically flat, oxide-free, low-carbon, gallium-rich surfaces.

2. Removal of the group V element: Removal of the group V element from the lattice is being investigated by reduction with H_2 to form a volatile hydride. The surface concentration of the group V element is decreased in order to facilitate the formation of the group III nitride. This step can also prevent a group V oxide from forming and reacting with the base semiconductor. Recently, Buhaenko et al, [7] found that heating in H_2 at 570^{0}K did produce GaAs with high gallium concentrations at the surface.

3. Nitridation of the metal-rich surface to form a large band gap semiconductor: In this step, the group III metal at the surface reacts

with hydrazine (N_2H_4) and produces a group III nitride.

4. Application of protective coating: The final step is the deposition of a hard, stable, insulating dielectric. Boron nitride has been chosen as the final dielectric because it has excellent passivating properties.[8-10] The deposition of boron nitride uses borohydride and hydrazine in a heterogeneous reaction.

REACTOR CONSTRUCTION

The reactor has been built to (1) operate under stringent safety procedures, (2) minimize oxygen and water contamination, (3) control the partial pressure of hydrazine in the carrier gas, (4) control pressure, temperature, and mass flow, (5) provide uniform distribution of reactants across the substrate surface, (6) allow mathematical modeling, (7) provide optimal film growth, and (8) dispose of byproducts and excess reactants.

The complete process diagram (Figure 1) involves three subsystems:

a) Feed gas system (Figures 2 & 3)
b) Reactor system (Figure 4)
c) Effluent Disposal system (Figure 5)

As shown in Figure 1, the reactant gases are purified and fed into the reactor. Anhydrous hydrazine (*Olin* ultra-pure, 98.5%) is vaporized by means of a temperature-controlled gas bubbler and fed into the reactor with a carrier gas. In the reactor, the gases and the substrate are heated with a tube furnace. The byproducts and unreacted gases exit the reactor and are treated in the effluent disposal system. The gas handling system is designed to isolate the argon carrier gas feed to the N_2H_4 bubbler so that no other gases can accidentally mix with the N_2H_4. The HCl line is also isolated except for one purge/vacuum line. All valves and fittings for the HCl line are isolated and vented in a gas cabinet. The feed gas system is shown in Figures 2 & 3. To minimize oxygen, water, and particle contamination in the reactant gases, high purity stainless steel tubing, VCR fittings, and ultra-high purity gases are used. Point-of-use purification for the gases is used to lower the oxygen and water content below 1 ppm.[11] An orbital arc-welder was used to make clean, leak-free butt welds. VCR fittings provide the highest level of purity for the gas delivery system.[12] However, VCR fittings could not

be used on the reactor chamber itself because of its size and the need for easy sample transfer. The chamber uses a o-ring gasket seals for the sample transfer door. Therefore, to minimize the contamination from the atmosphere, the reactor chamber is built into an nitrogen-filled dry box as shown in Figure 4. The water concentration is below 0.1 ppm, and the oxygen concentration is below 0.4 ppm. The dry box also serves as a safety containment chamber for the hydrazine during loading, use, and storage. Only materials approved for the transport and delivery of the gases are used. For example, Pyrex glass can be used to safely handle hydrazine.[13]

Pressure, temperature, and carrier gas flow rates are chosen as the control variables. The reactor can be operated at atmospheric or low pressure (<1 torr). Unfortunately, the vacuum leak-back rate of the o-rings in the reaction chamber is unacceptably high. Using a mass spectrometer and helium-leak test, a faulty valve and gasket seal were identified. The remainder of the reactor has a leak rate less than 1×10^{-9} scc/torr*sec. A minor design change to the gaskets and valves at the reactor entrance have been made and are being installed. Pressure control is particularly important when operating the reactor at a fixed reduced pressure while varying the gas flow rate and temperature. The current low-pressure control method uses a pressure meter and manual control. The system has been designed for easy upgrade to automatic pressure control. Producing a uniform temperature profile is difficult at the intermediate operating temperatures of this process (<500^{0}C). The reactor uses a Lindberg digital PID controller and a tube furnace to control the temperature. Figure 6 shows the setpoint verses actual temperatures measured with an IR probe, shielded thermometer, and wax-melt tests. Mass flow fluctuations are kept to a minimum by using sensitive Brooks and Tylan mass flowmeters, electric control valves, and Tylan analog controllers. Calibration of each flowmeter was checked by filling a known volume from vacuum. The vapor pressure of the hydrazine controls the concentration in the gas feed stream. The carrier gas flow rate through the hydrazine is controlled with a mass flow meter and valve, and the temperature is controlled with a constant temperature bath.

The core of the reactor is a 3" diameter Pyrex tube heated with the tube furnace. The design of the injector nozzle inside the tube is critical in the production of uniform films. [14,15] In the nozzle, the point of mixing for the hydrazine and borohydride is very important because an undesirable product can form, especially at low temperatures. [16] The current design in Figure 7 was made for ease of fabrication, and

operation. Some undesirable products do form at the mixing point in the tube. A higher velocity in the reaction tube is desirable. Future modifications will change the mixing point to the center of the reactor. Currently, the flow characteristics and film properties produced with the nozzles are being evaluated.

Lastly, the disposal system must be designed to safely dispose of the byproducts and excess reactants. Figure 5 shows the disposal system for atmospheric pressure operation. Oil acts as a filter removing any particulates and preventing air from entering the reactor. The excess hydrazine and related byproducts are disposed by reaction with sodium hypochlorite. Also, the excess HCl is neutralized with sodium hydroxide. Under low pressure conditions, the unreacted gases are decomposed with hot iron and copper before reaching the vacuum pump.

REACTOR MODELING

An isothermal equilibrium stage of a distillation column is used to model the N_2H_4 bubbler system. Heat is added to the bubbler and vaporizes the hydrazine. The carrier gas enters the bubbler, and transports the hydrazine vapors to the reaction chamber. The equations that govern this process are:

$$\text{Antoine Equation: } \ln P_i = A + B/T \tag{13}$$

$$\text{Equilibrium Equation: } y_i = P_i/P_t\ x_i \tag{14}$$

$$\text{Mass Balance: } y_i\ V_{in} - y_i\ V_{out} = x_i\ L \tag{15}$$

$$\text{Energy Balance: } H\ V_{in} - H\ V_{out} - hL + Q_{add} = 0 \tag{16}$$

where:

y_i = mass fraction in vapor phase
x_i = mass fraction in liquid phase
P_i = vapor pressure
A,B= Antoine coefficients
T = Temperature
P_t = Total Pressure
V_{in},V_{out} = Volumetric flow of gas
L = Liquid volume
H,h = Enthalpy of phase
Q_{add}= Heat added

Another crucial design feature in the reactor subsystem is the sample position. The exact position greatly affects the mathematical modeling. (17) By choosing simple geometries, the fluid flow and reaction chemistry can be uncoupled allowing useful models to be developed. The orientation chosen was a stagnation-point flow design. The general mathematical model developed involves equations of state, component

mass balance, axi-symmetric continuity, momentum, heat, and species balance equations. These equations describe transport of momentum, energy, and mass in the reactor and account for the velocity, temperature, pressure, and compositional effects on the reactions. The equations are being solved, and the results will be used to develop a kinetic model.

SUMMARY

The following tasks have been completed thus far in the project.

1. The design of process sequence is complete.
2. The design and construction of reactor is complete.

3. Reactor system has been helium-leak checked.
    a) Stainless system leak rate is less than
        1 x 10-9 scc/torr*sec.
    b) Glass reactor leak rate is poor.

4. The formation of group III and transition metal nitrides at atmospheric pressure is in progress.

5. Minor changes are being made to the system design.
    a) Improved valves and seals in the glass reactor will allow operation at reduced pressures.
    b) Redesign of the injector nozzle will decrease formation of undesirable products.

FUTURE WORK

Work will continue on the formation of the group III and transitional metal nitrides at atmospheric and low pressure conditions. Properties of the films will be evaluated with x-ray photoelectron spectroscopy or auger electron spectroscopy, capacitance-voltage measurements, and photoluminescence measurements.

REFERENCES

1. F. Capasso and G. F. Williams, Journal of Electrochemical Society, **129**, 821, (1982).

2. S. Singh, R. S. Williams, L. G. VanVitert, A. Schlierr, I. Camlibel, and W. A. Bonner, Journal of Electrochemical Society, **129**, 447, (1982).

3. N. Barbouth, Y. Berthier, J. Oudar, J. M. Moison, and M. Bensoussan, Journal of Electrochemical Society, **133**, 1663, (1986).

4. J. Saito and K. Kondo, Journal of Electrochemical Society, **137**, 1305, (1990).

5. J. Saito and K. Kondo, Journal of Applied Physics, **67**, 6274, (1990).

6. J. Saito and K. Kondo, Proceedings of the SPIE - The International Society for Optical Engineering, Multi-chamber and In-situ Processing of Electronic Materials, Santa Clara, CA, Oct. 1989, **1188**, 115, (1990).

7. D. S. Buhaenko, S. M. Francis, P. A. Goulding, and M. E. Pemble, Journal of Crystal Growth, **97**, 591, (1989).

8. B. Bayraktaroglu and R. L. Johnson, Journal of Applied Physics, **52**, 3515, (1981).

9. J. V. Dalton and J. Drobek, Journal of Electrochemical Society, **115**, 865, (1968).

10. A. B. Bhattacharyya and E. Lakshmi, Microelectronics Journal, **14**, 43, (1983).

11. T. Cambria and G. Tom, Solid State Technology, "Purification of Reactive Process Gas Streams", July 1989.

12. R. M. Cohen, Microcontamination, **8**, 41, (1990).

13. E. W. Schmidt, Hydrazine and its Derivatives, Wiley, New York, (1984).

14. W. Lee, Chemical Vapor Deposition of Dispersed Phase Ceramic Composites, Ph.D. Dissertation, Georgia Institute of Technology, January 1990.

15. J. L. Fitzjohn and W. L. Holstein, Journal of Electrochemical Society, **137**, 699, (1990).

16. A. Stock, Hydrides of Boron and Silicon, Cornell University Press, Ithaca, 1933.

17. C. R. Kleign, et al, Journal of Electrochemical Society, **136**, 3423, (1989).

FIGURE 1: COMPLETE SYSTEM

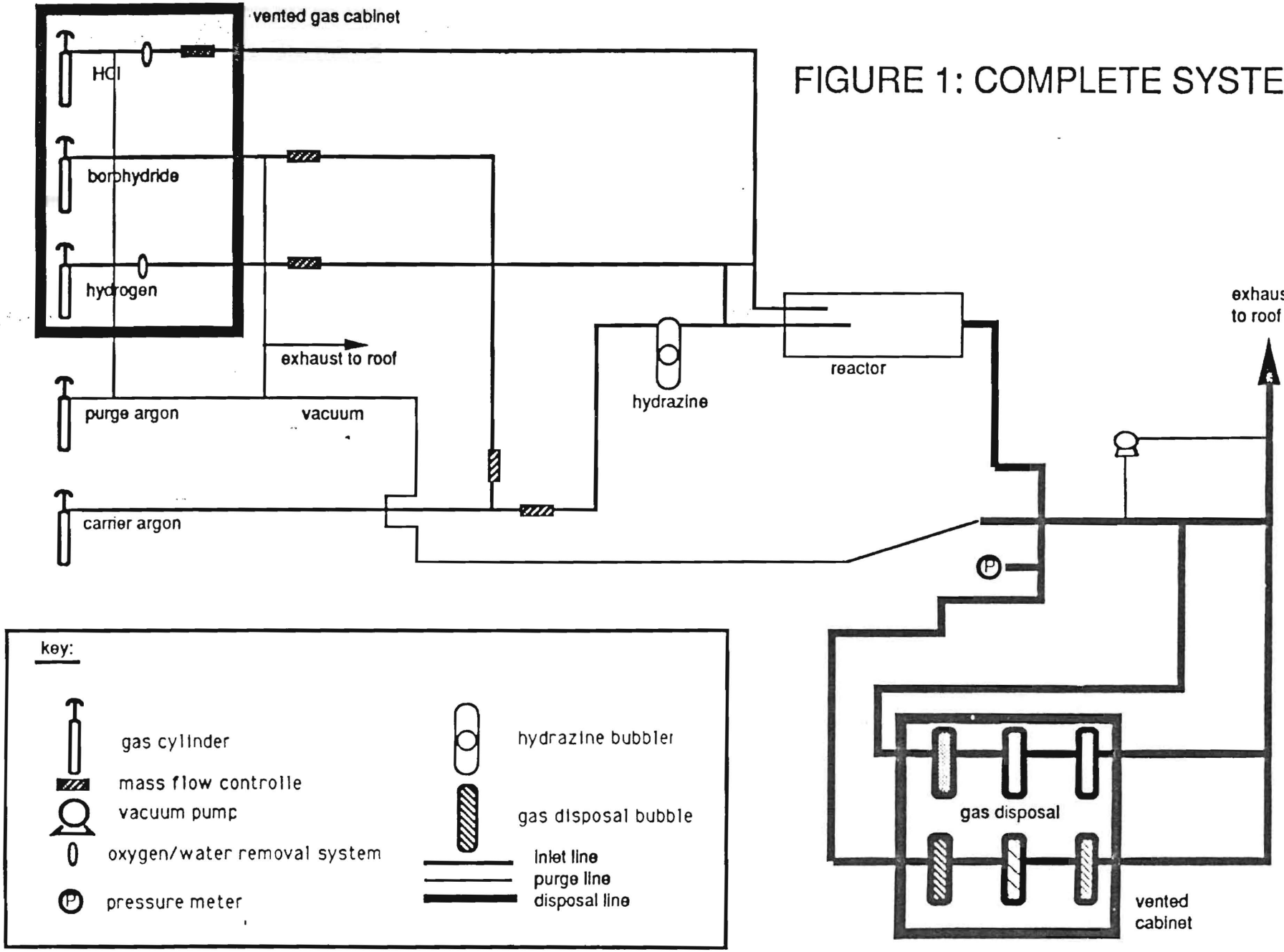

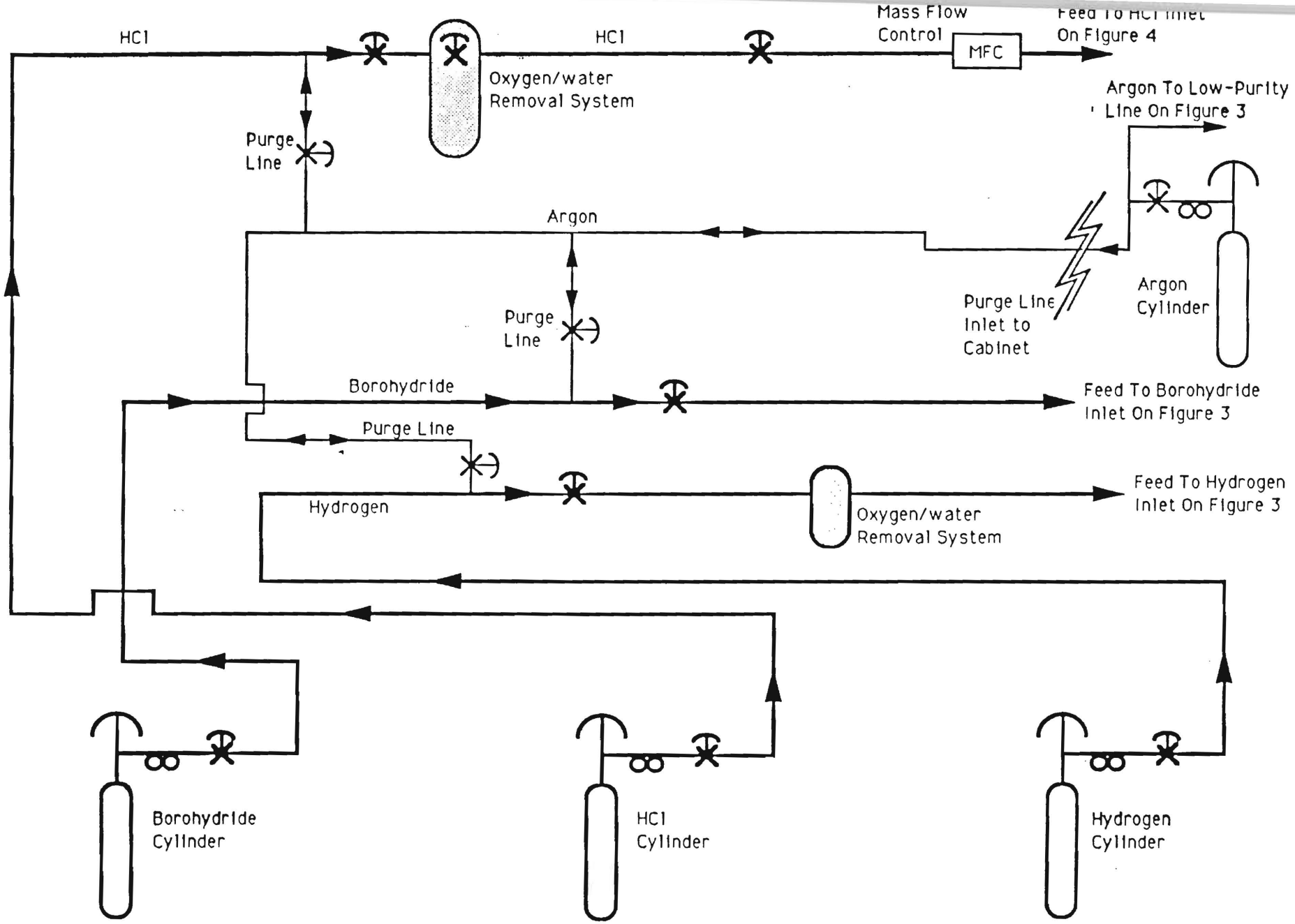

FIGURE 2 - PIPING SECTION 1

Piping section 1 is located inside a vented gas cabinet for safety.

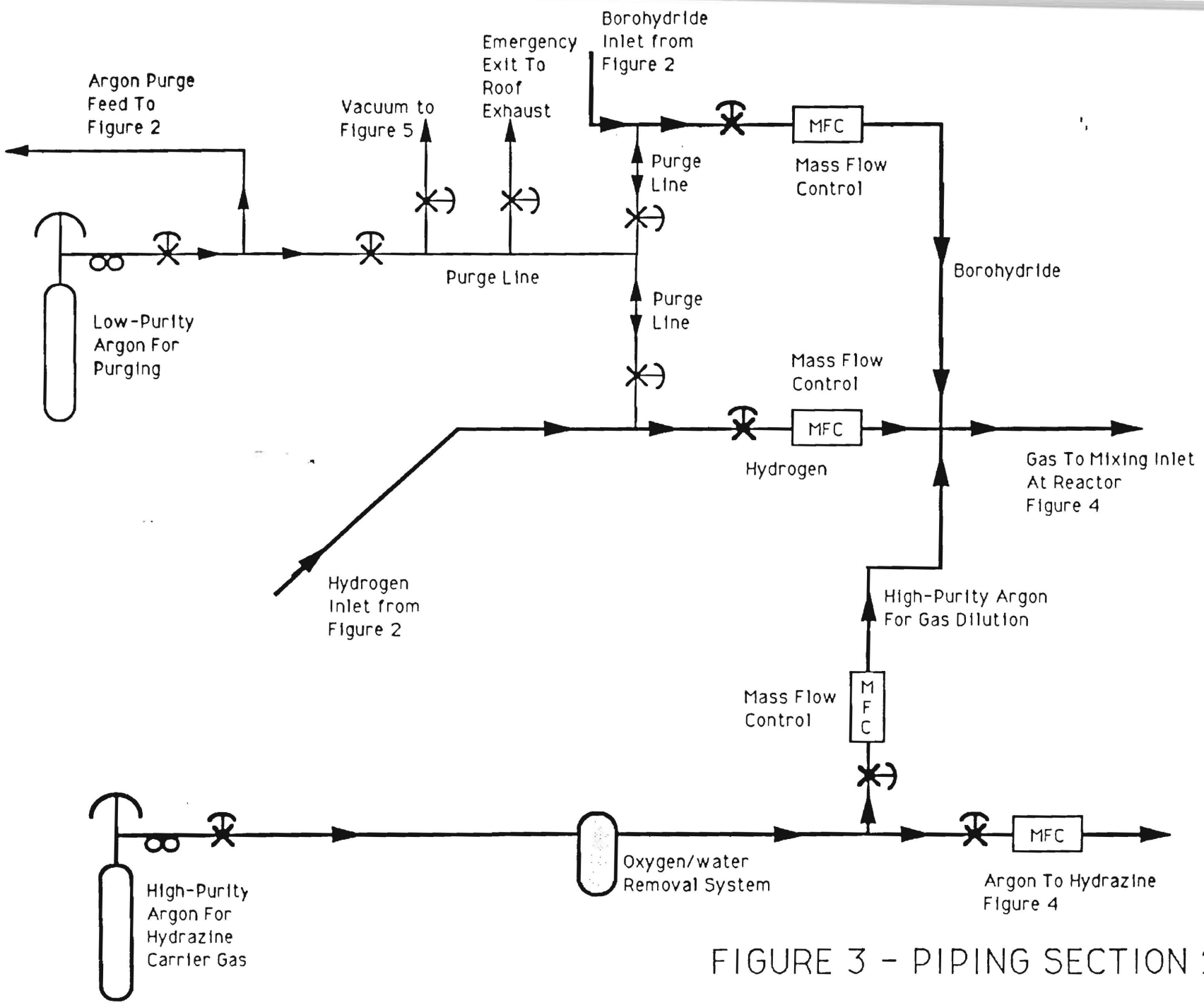

FIGURE 3 - PIPING SECTION 2

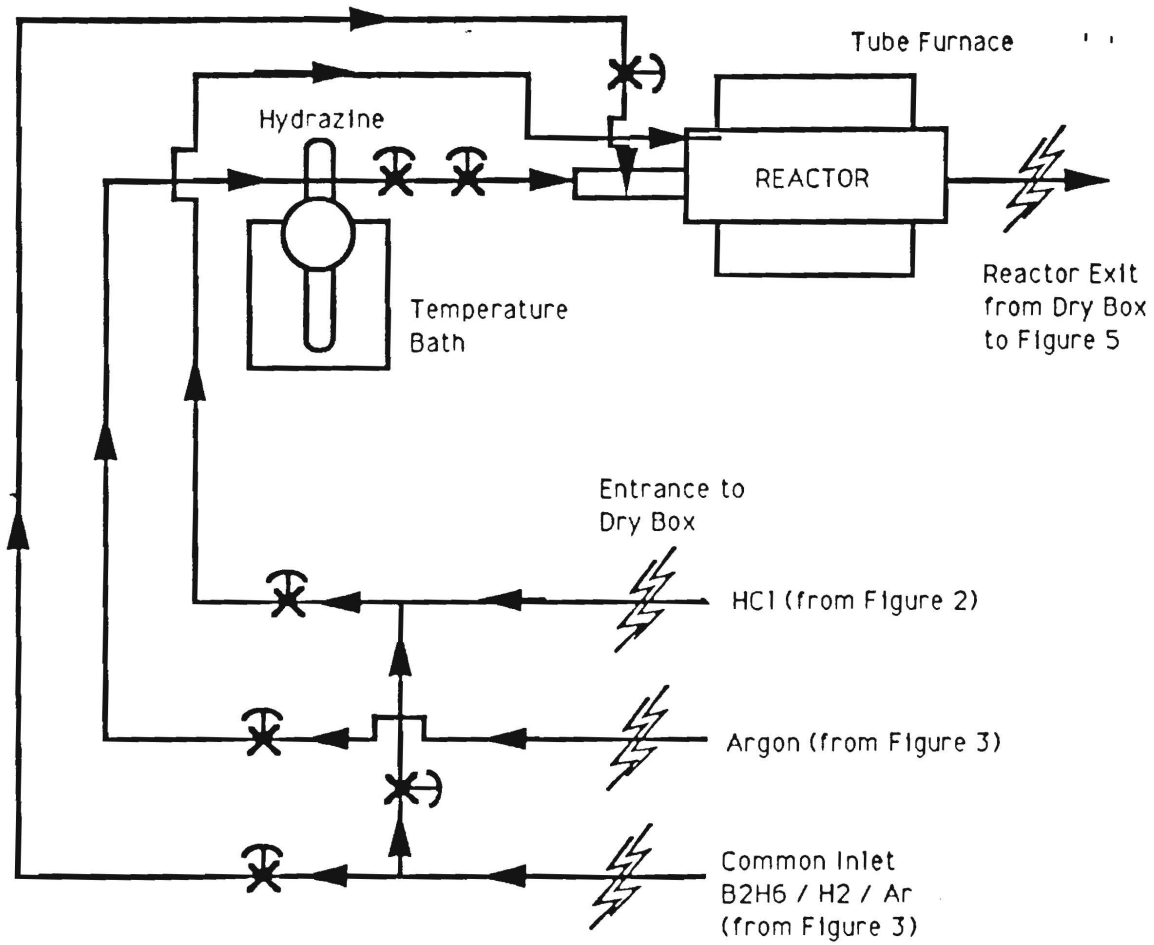

FIGURE 4 - REACTOR SYSTEM

This reactor system is encased in an inert gas dry box. This serves two purposes. First, hydrazine handling is much safer in an inert gas atmosphere. Second, competing reactions between the III-V compound and water and oxygen are minimized.

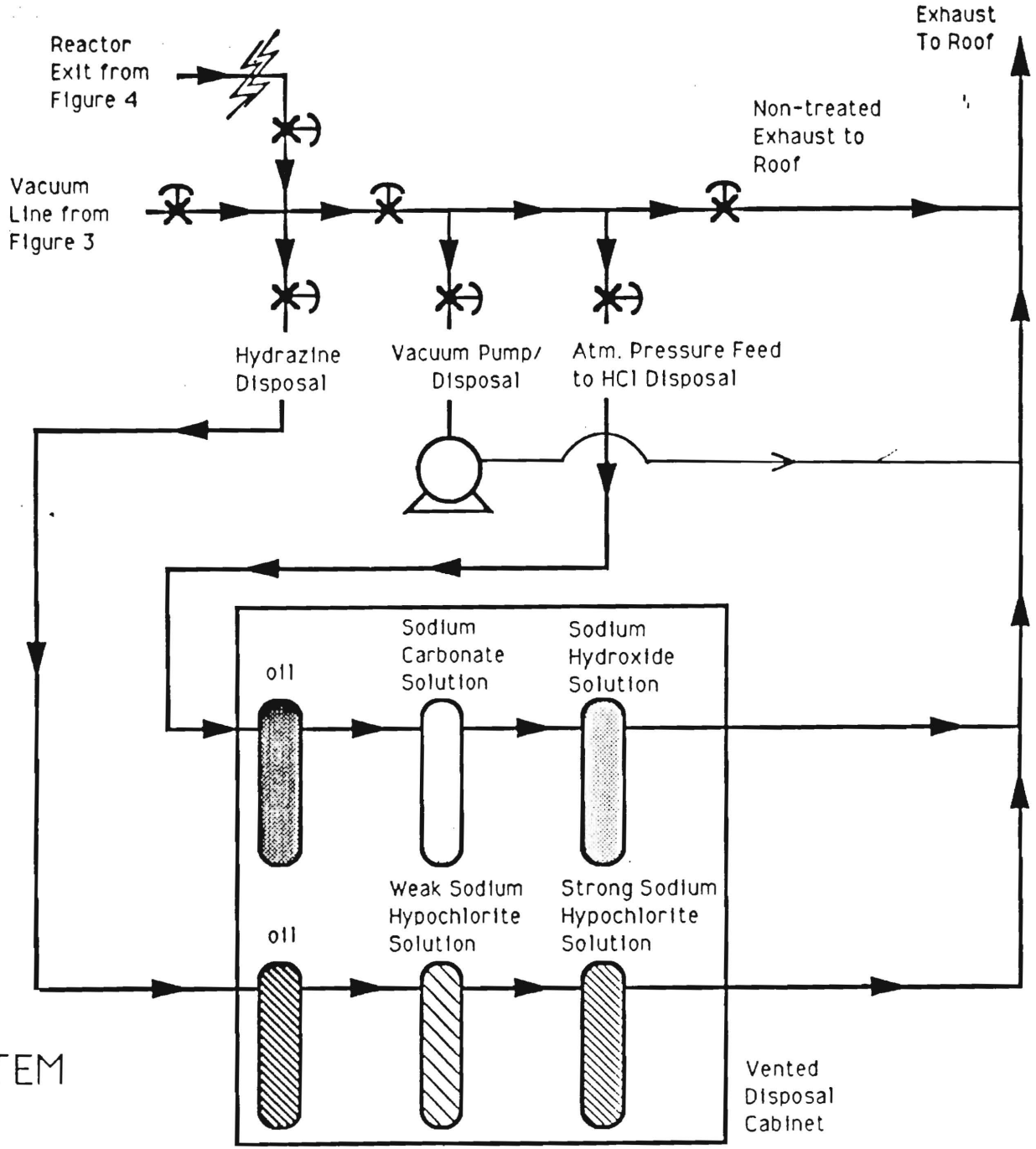

FIGURE 5
DISPOSAL SYSTEM

Figure 6

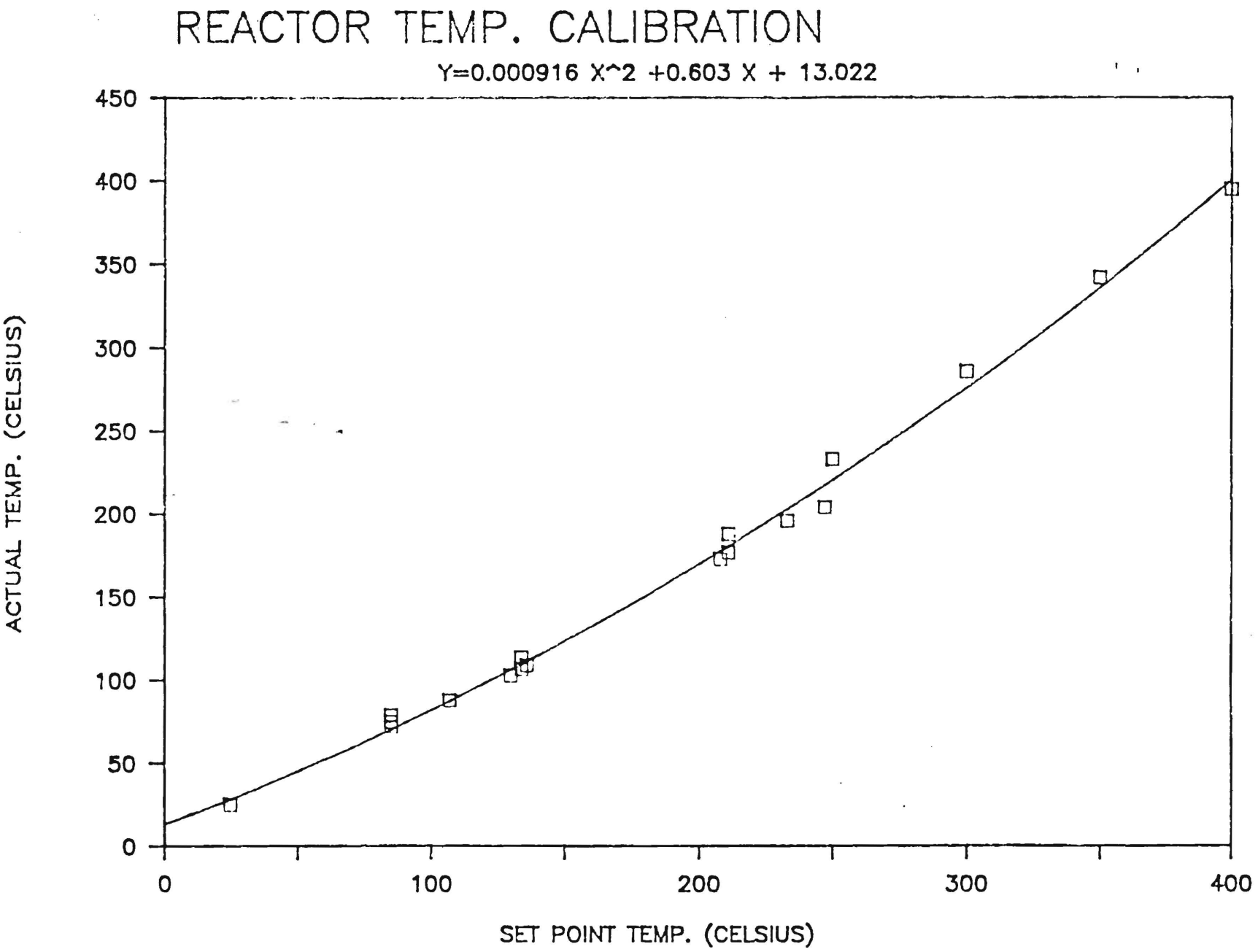
REACTOR TEMP. CALIBRATION
Y=0.000916 X^2 +0.603 X + 13.022
ACTUAL TEMP. (CELSIUS)
SET POINT TEMP. (CELSIUS)
0
50
100
150
200
250
300
350
400
450
0
100
200
300
400

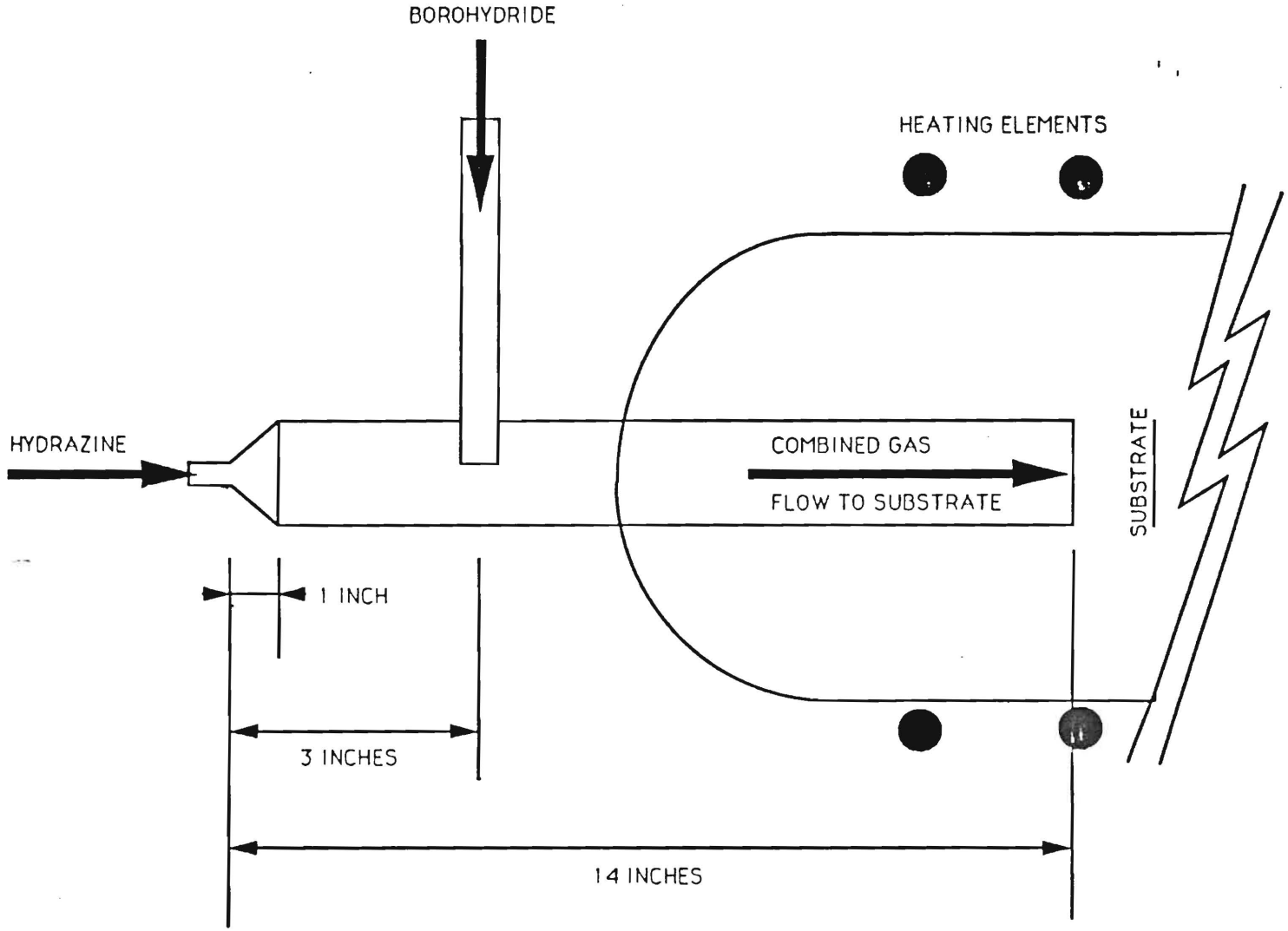

Figure 7

INJECTOR NOZZLE DESIGN

LOW TEMPERATURE CVD REACTOR FOR SEMICONDUCTOR AND METAL PASSIVATION

Final Report
September 15, 1992

Presented to:
Engineering Foundation
Air Force Engineering Research Initiation Grant
Contract RI-B-91-18

Prepared by:
Kirkland W. Vogt and
Dr. Paul A. Kohl
Georgia Institute of Technology
School of Chemical Engineering
Atlanta, Georgia 30332-0100

Table of Contents

LOW TEMPERATURE CVD REACTOR FOR SEMICONDUCTOR AND METAL PASSIVATION

1. SUMMARY:

A process has been developed to form nitrides at low temperatures on semiconductors (GaAs and Si), and transition metals (e.g. Fe, Ta). Reactive nitrogen species are generated by cracking hydrazine. The chemical vapor deposition of boron nitride has been demonstrated by the reaction of borohydride and hydrazine. A mathematical model of the reactor has been completed. The Record of Invention has been filed with the patent organization at the Georgia Institute of Technology.

Gallium nitride has been formed on GaAs by reaction of Ga with hydrazine (analogous to the growth of silicon dioxide on silicon) and expulsion of the As as a hydride. This is expected to lead to low surface state densities for the passivation of III-V compounds. The process has attracted considerable attention from IBM, and As capped samples provided by IBM will be nitrided and evaluated. Silicon nitride has been formed on Si. Capping the silicon with silicon dioxide prevented the formation of the nitride.

A survey of several transition metals has shown that nitrides can be formed by the use of hydrazine by converting the metal into the nitride or converting the metal oxide into the nitride. Iron oxide and tantalum oxide can be converted into at iron nitride and tantalum nitride, respectively. Nitride-like films were formed on Fe, Cr, Mn, Ti, V, Mo, W, and Ta.

In the CVD deposition of boron nitride from the reaction of borohydride and hydrazine, the temperature at the point of mixing is critical in determining the final composition of the film. Boron nitride is intended to be used as a capping material on the semiconductor samples.

Future work will continue along the above mentioned lines of work. Although a high purity reactor has been demonstrated, the purity of the hydrazine needs to be improved in order to lower the water content. The nitride passivated semiconductor samples will be characterized for surface state density. The reactions on InP and GaSb will be investigated. The quality of the metal films and use of nitrides as a passivation layer (i.e. iron nitride) will be investigated. Finally, the temperature of the hydrazine decomposition reaction will be lowered through the use of a catalyst. Funding for these projects is being solicited.

2. INTRODUCTION AND PROCEDURES:

The objective of this project was to demonstrate the production of nitride films at relatively low temperatures. The initial applications are for passivation of III-V semiconductors and devices, silicon devices, and the stabilization of transition metals.

The critical steps in the low temperature passivation of metals and semiconductors through the formation of nitride films are (1) the generation of reactive nitrogen species, (2) the removal of native oxides and contaminates to prevent the inclusion of defective interfaces (3) the removal of reaction products, and (4) the capping of the passivated layer with a suitable mechanical barrier.

The generation of reactive nitrogen intermediates in this project is based on the decomposition of hydrazine. The heat of formation of hydrazine is +38 kcal/mole, making its decomposition an exothermic process which can be catalyzed by numerous metals at temperatures as low as 2 ^{0}C. The reactor was designed and constructed with stainless steel, welded joints and a variety of ultra high purity gases for cleaning.

In the past year, the construction of the reactor has been completed. A nitride reaction sequence was developed to eliminate high temperatures (800-1000 °C), high-energy particles (plasmas), and oxygen and water impurities normally encountered in nitride formation. High temperatures can cause unwanted decomposition of metal and semiconductor substrates. High-energy particles can create undesirable crystalline defects in semiconductors. Secondary reactions with oxygen and water can create oxides. Group V oxides can undergo further reactions with the semiconductor substrate to produce undesirable conductive layers at the interface.[1]

The first step in the reaction sequence was to remove detrimental native oxides and carbon deposits with conventional clean/etch solutions.[2] After drying the sample with nitrogen, the sample was introduced into the reactor. The reactor was purged with 1000 sccm argon, and the temperature was increased. For III-V compounds, a second cleaning step using gas-phase HCl/H_2 reactions was investigated to further remove native oxides and increase the group III concentration at the surface. After the gas phase cleaning steps, the reactor was purged for 30-120 minutes. Next, the surfaces were reacted with anhydrous hydrazine (*Olin Ultra-pure*, 99.7%) to produce a metal nitride. In some cases a final CVD reaction with diborane and hydrazine was used to deposit a boron nitride protective coating.

3. RESULTS:

The results section will be broken into four parts; (1) the construction and modeling of the reactor, (2) transition metal nitrides, (3) semiconductor nitrides, and (4) boron nitride.

3.1 Reactor Construction and Modeling: The reactor has been designed and constructed with the following objectives; (1) to operate under stringent safety procedures, (2) minimize oxygen and water contamination, (3) control the partial pressure of hydrazine in the carrier gas, (4) control temperature and mass flow, (5) provide uniform distribution of reactants across the substrate surface, (6) allow mathematical modeling, (7) provide optimal film growth, and (8) dispose of byproducts and excess reactants safely. A discussion of the reactor construction was included in The Interim Report for Contract # RI-B-91-18, March 1, 1992. Mathematical modeling for the reactor has been completed and is discussed in Appendix 1.

3.2 Transition Metal Nitrides: Nitride formation on ten metals was attempted in order to investigate the general applicability of the process. Each metal was reacted separately to prevent cross contamination between samples. First, the metal samples were rinsed with 1,1,1-trichloroethane, acetone, and methanol for 30 seconds each to remove any carbon contaminants. The series was repeated a second time, and then the samples were rinsed with distilled water for one minute. The metal samples were then dipped in one of the following etch solutions for 30 seconds to remove the native oxide:

Fe, Cr, Mn	1 HCl / 2 H_2O
Ti, V, Mo, W	1 HF / 15 H_2O
Al	1 NaOH / 5 H_2O
Ta	1 HNO_3 / 1HF / 20 H_2O
Co	1 HNO_3 / 10 H_2O

The samples were rinsed with distilled H_2O for 1 minute and blown dry with nitrogen. After the sample was placed in the reactor, it was purged with 1000 sccm ultra high purity (UHP) argon. The reactor temperature was increased to 400 °C during the purge cycle. After 30 minutes, 1.3 sccm anhydrous hydrazine (99.7%) and 200 sccm UHP argon were fed into the reactor. The gases impinged on the metal sample in the center of the hot zone of the reactor. After 1 hour, the hydrazine flow was stopped, and the reactor was cooled and purged with 1000 sccm UHP argon for 30 minutes. The sample was removed and stored in a dry box maintained at less than 1 ppm oxygen and less than 1 ppm water until they could be analyzed.

The surface composition was determined by Auger Electron Spectroscopy (AES) and/or X-ray Photoelectron Spectroscopy (XPS). AES results showed metal-nitrogen-oxygen films were made with Fe, Cr, Mn, Ti, V, Mo, W, Ta, and Co. In all cases, the films contained

more nitrogen than oxygen in the bulk of the film. XPS results showed that the nitrogen in the Ta and V films was in the form of a nitride and not the nitrite or nitrate oxidation state. Also, the metal was in the metal-nitride oxidation state. XPS experiments for the other samples are in-progress. These results illustrate the versatility of the metal-nitride reaction sequence using hydrazine.

Three metals were chosen for more detailed experiments; Fe, Ta, and Co. In the first set of experiments, different cleaning solutions were chosen to remove the native oxide films. For Fe and Co, 10 % HNO_3 was used for 2.5 minutes, and for Ta, 10% anhydrous HF in methanol was used for 5 minutes. The remainder of the cleaning sequence described above was used. The etched samples were compared to a second set of samples where a thick oxide film was grown by heating the samples in air at 400 °C for 7 to 12 minutes. Both sets of samples were treated with hydrazine at 400 °C for 1 hour. AES was used to analyze the nitride films and compare them to control samples which received no hydrazine treatment.

First, reacting the chemically etched and the pre-oxidized iron samples with hydrazine produced layered films with similar nitride compositions. The film was composed of iron, nitrogen, and oxygen at the surface and primarily iron and nitrogen near the metal-film interface. The AES profile for the hydrazine treated chemically etched iron samples shows that the total thickness of the film (oxide plus nitride) is greater than the film thickness for the control sample. The pre-oxidized film was thinner for hydrazine-treated Fe than for the control samples.

These results suggest several conclusions. First, oxide reactions due to residual water in the hydrazine compete with nitride reactions during hydrazine treatment. Second, hydrazine reacts directly with elemental Fe to produce an iron nitrogen compound at the film/metal interface. The nitrogen-iron species is believed to be iron nitride. Lastly, because the thickness of the oxidized film appears to decrease with hydrazine treatment, it indicates that the oxide film is chemically converted onto the nitride. This experiment shows the need for more extensive drying of the hydrazine.

Second, the hydrazine treatment of the chemically etched Ta samples produced tantalum-nitrogen-oxygen films with the nitrogen concentration greater than the oxygen concentration. The nitrogen compound has the same XPS signature as tantalum nitride. The control sample shows however, that oxygen is introduced with the N_2H_4 treatment. Hydrazine treatment of the pre-oxidized Ta produced thinner oxide films (compared to control) and produced Ta-nitrogen-oxygen films on the surface. The film was essentially all oxide at the film-metal interface indicating that nitride conversion of the metal had not taken place, probably because the reactants had not diffused to the interface. These results also suggest that N_2H_4 reacts with the oxide and converts it to the nitride.

Third, interesting results were found for cobalt. For both the chemically etched and pre-oxidized Co, a layered film was produced. A

cobalt-oxygen rich film was found at the surface. A thick cobalt-nitrogen film was found under the oxide film at the film/metal interface. XPS results showed that the nitrogen was in the form of an amine. This was expected because cobalt nitride cannot be formed.[3] The oxide thickness was larger for the chemically etched, N_2H_4 treated samples than for the control showing that additional oxide had been formed during the hydrazine treatment. However, the oxide thickness appears to be smaller for N_2H_4 treated pre-oxidized samples than the control samples. This suggests that the hydrazine treatment is able to reduce oxide thickness of the cobalt samples, or that the sputtering rate of the nitride film is faster than that of the oxide film. Thirdly, the hydrazine reactant is able to diffuse through the oxide to react directly with the elemental cobalt.

Metal Summary: These survey samples are very interesting for several reasons. First, nitride films can be made from both chemically etched and pre-oxidized transition metals. In the case of Fe and Ta, hydrazine reacts with the oxide and forms nitride or amine compounds in the oxide films. For Fe and Co, hydrazine reacts directly with the metal. Both results need further study to identify the mechanisms. Current efforts will focus on removing the 0.3% H_2O from the anhydrous hydrazine. This could further minimize the competing oxide reactions.

3.3 Semiconductors:

3.3.1 Silicon: The nitride reaction sequence with hydrazine was investigated with silicon and gallium arsenide (GaAs). For silicon, the same pre-treatment steps as described with the metals were used. The samples were cleaned with 1,1,1-trichloroethane, acetone, methanol, and distilled water. Next, they were etched in 10% HF to remove the native oxides. After introduction into the reactor, argon purging, and ramping the temperature to 400 ^{0}C, the samples were exposed to 1.3 sccm N_2H_4 for 1 hour. An oxidized sample (515 A SiO_2) was also exposed to hydrazine for 1 hour at 400 ^{0}C.

The films formed on Si were evaluated with XPS and AES. The AES results show that a silicon-nitrogen-oxygen film formed on the etched samples. No nitrogen was found on the silicon dioxide samples indicating that silicon dioxide is not converted into the nitride. XPS results show that the oxidation state of the nitrogen was the same as that of a nitride and the oxidation state of the silicon was that of silicon nitride and silicon dioxide. Just as with the metal samples, the results suggest that competing oxide and nitride reactions are occurring. However in this case, the hydrazine does not react with silicon dioxide, and the active nitrogen species do not diffuse through the dense oxide to react with the elemental silicon.

3.3.2 Gallium Arsenide: A reduced factorial experiment was used for GaAs to evaluate the reaction sequence. The following chart shows the variables used.

Variable	Level A	Level B
a) wet clean 30 sec. each	10% HCl/propanol 10% HF/methanol	1/1/10 $H_2SO_4/H_2O_2/H_2O$
b) 2% Br/methanol etch	30 sec. dip	60 sec. rub
c) HCl gas etch	1% in H_2	20% in H_2
d) post-clean purge	Ar; 30 min.	H_2; 2 hours
e) temperature	300 °C	400 °C

The results of the GaAs reduced factorial experiment were very interesting. For one of the samples (1/1/10 $H_2SO_4/H_2O_2/H_2O$ clean, 30 second Br/methanol rub, 1% HCl gas-phase clean, 30 minute argon purge, and 400 °C temperature), a thick orange-yellow-red rainbow colored film was formed. Prochazkova et al [4] also described their GaN films as yellow-orange in color. An AES depth profile is shown in Figure 1. It shows that the film is a mixture of gallium, nitrogen, oxygen, chlorine, and sulfur. A very important result is that most of the arsenic has been removed. The oxidation state of the nitrogen is the same as that of a nitride. Another important observation is the increase in the nitride concentration at the GaN/GaAs interface, which is electrically the most important region of the film. A control sample which had not been exposed to hydrazine was also analyzed. The AES profile shows that the oxygen film on the control was much thinner than on the treated sample. These results suggest that direct nitridation of GaAs has occurred and that arsenic has been removed, most likely as a hydride. The results also indicate that competing reactions between water and hydrazine exist, and cleaning steps can incorporate impurities into the film.

The XPS analysis shows that the nitrogen in the film on GaAs was in the nitride oxidation state and gallium was in the gallium nitride oxidation state. Initial results for the reduced factorial design experiment used the intensity of nitrogen XPS signal at the surface as an evaluation tool. It shows that Br-methanol rub, 1% HCl gas phase clean and 400 °C produce more nitrogen at the surface. It also shows that nitrogen is in the nitride oxidation state. Further evaluation of the reduced factorial design experiments are in progress.

To summarize, the results for the GaAs experiments show that (1) nitride films can be made on GaAs below 400 °C, (2) arsenic is removed from the films, (3) competing reactions between water and nitrogen exist, (4) cleaning steps can incorporate impurities into the

films, (5) cleaning steps can effect the growth rate, and (6) higher temperatures increase the nitride formation rate.

3.4 Boron Nitride Films:

The CVD deposition of boron nitride was attempted by reacting diborane with hydrazine. The purpose of the boron nitride is to form a thick mechanical protection barrier on top of the passivated material. Brown and white deposits were formed on the reactor walls under a variety of conditions. Some of these products formed are undesirable because the reactants are depleted before reaching the target sample. The brown deposit was most likely boron from diborane decomposition. The white deposit was thought to be a polymeric adduct of hydrazine and diborane. The purpose of the experiments and literature search was to investigate the effects of temperature on diborane and diborane/hydrazine mixtures. Three sets of reactor conditions were investigated.

3.4.1 Experimental:

3.4.1a Boron Nitride Deposition: Diborane (781 ppm in UHP argon; 500 sccm) and hydrazine (1.3 sccm) were mixed in a one inch tube outside the reactor. The mixture was warmed and directed into the main reactor where it impinged on a gallium arsenide sample for 1 hour. The temperature in the mixing zone has not been measured. The temperature in the center of the main reactor was 400 °C.

3.4.1b White Film Formation: A concentric injection tube was used to mix the hydrazine and diborane after reaching the center of the main reactor. The reactor was first purged with 1000 sccm UHP argon for 15 minutes. Next, hydrazine was fed into the center tube at 1.3 sccm, and 500 sccm UHP argon was fed into the outer concentric tube. Lastly, the hydrazine was fed into the center tube at the same concentration and flow rate while diborane was fed in the outer concentric tube at 781 ppm in 500 sccm UHP argon. The tubing outside the main reactor was warmed with heat tape to prevent condensation of hydrazine on the glass tubing. Pyrex glass tubes were used as samples for film deposition at the concentric tube exit. New samples were collected in the center of the main reactor at 29, 50, 100, 150, and 200 °C.

3.4.1c Diborane Decomposition and Decaborane: Again the concentric tube setup was used. The reactor was purged with 1000 sccm argon for 15 minutes. Next, diborane (781 ppm in UHP argon at 500 sccm) was fed into the outer tube. No hydrazine was present in the reactor. The heat tape was not used on the endcap during this investigation. Because decaborane melts at 99.5 °C, it was hoped any decaborane formed would deposit on the endcap. The temperature in the center of the main reactor was varied from 80, 100, 150, 200, and

400 °C while observing the film deposition on the sample tube and endcap.

3.4.2 Results of the Boron Nitride Experiments: The results for each experimental setup are summarized below.

3.4.2a Boron Nitride: XPS confirmed that a boron nitride film was made at 400 °C. The XPS depth profile is shown in Figure 2. The binding energies for the boron 1s and nitrogen 1s peaks identified the oxidation states as boron nitride.[5] During the deposition, a brown deposit was made where heat tape covered the diborane inlet. White deposits formed on areas of the glass mixing zone which were not covered with heat tape.

3.4.2b White Deposit: The results below show that a white deposit will form below 200 °C.

Temp	Reaction Period	Film Appearance
29 °C	10 minutes	White on sample and main chamber
50 °C	10 minutes	White; same appearance as 29 °C
100 °C	10 minutes	White; same appearance as 29 °C
150 °C	60 minutes	White; not as thick as lower temperatures
200 °C	60 minutes	Brown prior to hydrazine mixing point; none after diborane and hydrazine mix

The 200 °C sample is interesting because it suggests that a hydrazine/diborane mixture does not form a white solid at 200 °C. Assuming that the brown film is boron, the sample also suggests that hydrazine is not diffusing upstream into the outer concentric tube at these flow rates.

3.4.2c Brown Film and Investigation of Decaborane Deposition: The results shown below suggest that a brown film will form from diborane above 200 °C. They also suggest that decaborane is not being formed.

Temp	Time	Film on Sample	Film on Endcap
88 °C	10 min.	None	None
100 °C	23 min.	None	None
150 °C	30 min.	None	None
200 °C	30 min.	Brown on sample	None
400 °C	60 min.	Brown on injector	None

The color and appearance of the 200 °C film was the same as the brown film on the 200 °C sample in the previous experiment. This helps support the hypothesis that the brown film comes from diborane decomposition. The 400 °C film was only slightly soluble in concentrated nitric acid and etched from the glass slowly.

3.4.3 Boron Nitride Conclusion: These results suggest the following conclusions.

1. Boron nitride can be deposited from hydrazine and diborane at 400°C.

2. A white deposit will form from a hydrazine and diborane mixture when the temperature is between 25 and 2000°C.

3. Significant decomposition of diborane occurs above 200°C.

4. Decaborane formation was not evident.

Qualitatively the results agree with others' found in literature. A Lewis acid-base reaction can occur between the electrophilic diborane and the nucleophilic hydrazine. These reactions often lead to a large number of ionic and covalent complexes and adducts.[6] Experimentally, diborane and hydrazine have been shown to form adducts below 200 °C.[7,8,9]

At higher temperatures, the adducts discussed above can undergo rearrangement to form different compounds. Hydrogen evolution often accompanies the rearrangement reactions. For example, ammonia-diborane adducts decompose at 200 °C to yield the ring-like borazine ($B_3N_3H_6$) and other products. Excess diborane favors the production of $NH_2B_2H_5$ while excess ammonia favors the

production of $B_2(NH)_3$.[10] Likewise, hydrazinolysis of aminoboranes with free hydrazine can yield ring-like and other addition compounds.[11]

In other studies, diborane decomposition has been investigated for boron deposition[12,13,14], polyhedral expansion of boron hydride chains[15], and exchange reactions between hydrogen and diborane[17].

4. Conclusions:

Hydrazine can be used to form nitrides on semiconductors, transition metals and by reaction with borohydride. A CVD reactor has been designed, constructed and modeled to deliver hydrazine and dispose of its by-products.

For transition metals, hydrazine can react directly with metal oxides or metals to produce nitride films. Diborane and hydrazine CVD reactions produce boron nitride films at 400 °C. Hydrazine can react with cleaned silicon surfaces produce silicon nitride films. Oxidized silicon surfaces do not react with hydrazine to produce silicon nitride. Gallium nitride films can be made from thermal nitridation of GaAs with hydrazine. Arsenic is removed from the GaN films during the nitridation reaction. Competing reaction between oxygen (or water) and hydrazine exist emphasizing the need to lower oxygen contamination.

5. Future Work:

Activated alumina will be used to reduce the water content of the hydrazine below its present 0.3% H_2O. A residual gas analyzer will be added to the reaction chamber to more closely examine the reaction products.

The passivated films on GaAs and Si will be characterized for thermal stability, photoluminescence, and surface state density. The reaction sequence will also be used to form nitride films on InP and GaSb. Arsenic-capped GaAs from IBM will be used to produce an oxide-free GaAs surface to react with hydrazine.

Corrosion tests on the transition metal nitrides will be performed to evaluate the quality of the nitride films. FT-IR will be used to gain molecular bonding information.

Bibliography:

[1] F. Capasso and G. Williams, Journal of Electrochemical Society, **129**, 821, (1982).

[2] S. Singh, R. Williams, L. VanVitert, A. Schlierr, I. Camlibel, and W. Bonner, Journal of Electrochemical Society, **129**, 447, (1982).

[3] Cotton and Wilkinson, Advanced Inorganic Chemistry, Third Edition, Interscience (1972).

[4] O. Prochazkova and F. Srobar, Kristall and Technik, **12**, 12, 1977, p. 1293-1302.

[5] Handbook of X-Ray Photoelectron Spectroscopy, Physical Electronics, Eden Prarie, MN (1980).

[6] Coyle and Stone, Progress in Boron Chemistry Vol. 1, 1964, Steinberg & McCloskey, pg 84-85

[7] J. Goubeau and E. Richter, Z. anorg. allg. Chem., **310**, 123, 1961.

[8] K. Niedenzu & J. Dawson, Boron-Nitrogen Compounds, Academic Press, NY, 1965, p. 76-77.

[9] A. Noth, Progress in Boron Chemistry, Vol. 3, R. Brotherton and H. Steinberg (editors), Peragomon Press, NY, 1970, p. 217.

[10] A. Stock, Hydrides of Boron and Silicon, 1933, p. 92-95.

[11] K. Niedenzu and J. Dawson, Boron-Nitrogen Compounds, Academic Press, NY, 1965, p. 76-77.

[12] J. Bauer, Progress in Boron Chemistry, Vol. 2, R. Brotherton and H. Steinberg (editors), Peragomon Press, NY, 1970, p. 240-241.

[13] R. Clarke and R. Pease, J. Amer. Chem. Soc., **73**, 2132, 1951.

[14] J. Bragg, J. Amer. Chem. Soc., **73**, 2134, 1951.

[15] S. Shore, Boron Hydride Chemistry, E. Muetterities (editor), Academic Press, NY, 1975, p. 148.

[16] T. Fehlner, Boron Hydride Chemistry, E. Muetterities (editor), Academic Press, NY, 1975, p. 177-185.

[17] J. Rigden and W. Koski, J. Amer. Chem. Soc., **83**, 3037, 1961.

[18] H. Schlichting, Boundary Layer Theory, McGraw-Hill, New York, (1987).

[19] K. F. Jensen, Microelectronics Processing: Chemical Engineering Aspects, American Chemical Society, (1989).

[20] P. J. Roksnoer, C. Van Opdorp, J. W. F. M. Maes, M. DeKeijser, and C. Weber, Journal of Electrochemical Society, **136**, 2427, (1989).

[21] S. Rhee, J. Szekely, and O. J. Ilegbusi, Journal of Electrochemical Society, **134**, 2552, (1987).

[22] L. J. Giling, Journal of Electrochemical Society, **129**, 634, (1982).

[23] W. G. Breiland and G. H. Evans, Journal of Electrochemical Society, **138**, 1806, (1991).

[24] R.B. Bird, W.E. Stewart, and E.N. Lightfoot, Transport Phenomena, Wiley, New York, (1960).

[25] S. Whitaker, Introduction to Fluid Mechanics, Robert E. Krieger Publishing Co., Malabar, Florida, 1968.

[26] M.E. Coltrin, R.J. Kee, and G.H. Evans, Journal of Electrochemical Society, **136**, 819, (1989).

[27] H. Schlichting, Boundary Layer Theory, McGraw-Hill, New York, (1987).

[28] J. W. Gauntner, J. N. B. Livingood, and P. Hrycak, NASA TN D5652, (1970).

[29] C. R. Kleign, etal., Journal of Electrochemical Society, 136, 3423, (1989).

[30] M. T. Scholtz and O. Trass, AIChE Journal, 16, 82, (1970).

[31] M. Michaelidis and R. Pollard, Journal of Electrochemical Society, 131, 860, (1984).

[32] K. F. Jensen, Microelectronics Processing: Chemical Engineering Aspects, American Chemical Society, (1989).

[33] R. B. Bird, W. E. Stewart, and E. N. Lightfoot, Transport Phenomena, Wiley, New York, (1960).

[34] JANAF Thermochemical Tables, Published bu U. S. National Bureau of

Standards, Washington D.C., NSRDS-NBS 37 (1971).

[35] D. W. Marquardt, SIAM Journal, 11, 431, (1963).

Appendix 1

Mathematical Modeling

Mathematical models for CVD, in combination with appropriate experiments, can lead to an increased understanding of the CVD chemistry. The areas of study could include homogeneous kinetic mechanisms, heterogeneous kinetic mechanisms, multi-component diffusion effects, thermo-diffusion effects, and complex fluid flow effects. By choosing simple geometries, the fluid flow and reaction chemistry can be uncoupled allowing useful models to be developed. Classic examples of possible geometries where exact solutions to momentum transport equations are known include: [19]

1. two-dimensional plane wedge
2. impinging jet
3. two-dimensional flow over a flat plate
4. infinite-radius rotating disk
5. stagnation point flow

All five examples require that at least one of the geometries be of infinite dimensions. For examples 1, 2, and 3, it is physically difficult to construct a reactor with these flow designs and obtain the uniform depositions required for microelectronics. Additionally, for example 2, high mass flow rates can cause the reactor walls to change the flow patterns and result in asymmetric vortexes and non-uniform deposition.[19, 20] For example 3, the reactor walls can create longitudinal convection rolls and other flow disturbances causing non-uniform deposition. [21, 22] For example 4, the flow pattern and deposition uniformity are very good [23], but the construction of the rotating mechanism inside a dry box is too difficult.

Thus, the orientation chosen was a stagnation point flow design. Fundamentally, chemical vapor deposition (CVD) reactions involve gas-phase and surface reactions combined with transport processes. CVD mechanisms involve a series of transport, adsorption, reaction, and desorption schemes. Similar reaction sequences are used for catalytic combustion, solid-fuel combustion, and heterogeneous catalysis. General mathematical models developed for CVD reactors involve sets of partial differential equations and boundary conditions. These equations describe transport of momentum, energy, and mass in the reactor and account for the temperature, pressure, and compositional effects on transport properties. Solution of these equations provide velocity, pressure, temperature, concentration, and reaction chemistry information. Several assumptions can be made which simplify the problem.

1. Gases are Newtonian fluids. [24]
2. The gases act as incompressible fluids. This assumption is valid if

the Mach number is much less than one. [24] The proposed Mach number is of the order 1×10^{-4}.

3. The system achieves steady-state quickly.

4. The gas flow is axisymmetric and irrotational. This assumption allows the velocity to be approximated as a function of the r and z directions only.

5. The gases behave ideally.

6. Horizontal orientation eliminates gravity effects in the momentum equations.

7. Viscous heating effects are negligible because the gas viscosity is very small.

8. Because the reactor is heated from the exterior (and thus nearly isothermal), thermo-diffusion effects are neglected.

9. The homogeneous and heterogeneous reactions do not contribute significant amounts of heat to the reactor.

10. Because the growth rate is small compared to gas flow rate, a no-slip assumption at the wafer surface boundary is used.[26]

The governing equations are:

equation of state: $$\rho \cdot R \cdot T = M \cdot P \tag{1}$$

continuity: $$\frac{\partial u}{\partial r} + \frac{u}{r} + \frac{\partial w}{\partial z} = 0 \tag{2}$$

u-momentum: $$u \cdot \frac{\partial u}{\partial r} + w \cdot \frac{\partial u}{\partial z} = -\frac{1}{\rho} \cdot \frac{\partial P}{\partial r} + \nu \left(\frac{\partial^2 u}{\partial r^2} + \frac{1}{r} \cdot \frac{\partial u}{\partial r} + \frac{u}{r^2} + \frac{\partial^2 u}{\partial z^2} \right) \tag{3}$$

w-momentum: $$u \cdot \frac{\partial w}{\partial r} + w \cdot \frac{\partial w}{\partial z} = -\frac{1}{\rho} \cdot \frac{\partial P}{\partial z} + \nu \left(\frac{\partial^2 w}{\partial r^2} + \frac{1}{r} \cdot \frac{\partial w}{\partial r} + \frac{\partial^2 w}{\partial z^2} \right) \tag{4}$$

heat equation: $$\rho \cdot C_p \cdot \left(u \cdot \frac{\partial T}{\partial r} + w \cdot \frac{\partial T}{\partial z} \right) = k \cdot \left(\frac{1}{r} \cdot \frac{\partial}{\partial r} \left(r \cdot \frac{\partial T}{\partial r} \right) + \frac{\partial^2 T}{\partial z^2} \right) \tag{5}$$

Species balance equations:

$$u \cdot \frac{\partial x_i}{\partial r} + w \cdot \frac{\partial x_i}{\partial z} = D \cdot \left(\frac{1}{r} \cdot \frac{\partial}{\partial r} \left(r \cdot \frac{\partial x_i}{\partial r} \right) + \frac{\partial^2 x_i}{\partial z^2} \right) - \sum_j a_{ij} \cdot N_i \tag{6}$$

Component balance: $$\sum_i x_i = 1 \tag{7}$$

where:

ρ = density, gm/cm^3
R = gas constant, 8.314 x 10^7 g cm^2/g-mole sec^2 ^oK
T = temperature, ^oK
M = average molecular weight gm/gmol
∂ = partial derivative
r = radial coordinate, cm
z = axial coordinate, cm
u = velocity in radial direction, cm/sec
w = velocity in axial direction, cm/sec
P = pressure, gm/cm sec^2
ν = kinematic viscosity, cm^2/sec
C_p = heat capacity, cal/gm ^oK
k = thermal conductivity, cal/cm sec ^oK
x_i = mass fraction of component i
D = diffusivity, cm^2/sec
N_i = homogeneous reaction rate, sec^{-1}
a_{ij}= stoichiometric coefficients

The boundary conditions are:

At **z = 0**: $u = 0$ (8)

$w = 0$ (9)

$T = T_s$ (10)

$$D \cdot \frac{\partial x_i}{\partial z} = -\sum_j a_{ij}^s \cdot N_i^s \quad (11)$$

At **z = ∞**:

$u = 0$ (12)

$w = -V$ (13)

$T = T_{bulk}$ (14)

$x_i = x_{io}$ (15)

where:

N_i^s = heterogeneous reaction rate of i^{th} species, cm/sec
V = free stream velocity, cm/sec

The velocity problem was first solved by Prandtl and Homann in the

early 1900's and appears in Schlichting. [27] More extensive research was performed in the 1960-70's; a literature survey appears in Gauntner, et al. [28] Presently, many workers have solved this problem for the impinging jet CVD reactor; for references see Kleign, et al. [29] A summary of the solution will follow.

Several assumptions are used in the solution:

1. When r/d is less than or equal to 1, the local mass transfer rate in the stagnation region is independent of the radial position. [30]
2. The area of diffusion is confined to an area where the boundary layer thickness is uniform.
3. The reactor diameter is large enough that the effect on the flow boundary is negligible.
4. The fluid flow outside the stagnation region (boundary layer) can be described by inviscid flow theory. Flow theory inside the boundary layer is described by viscous flow theory. Thus, for the inviscid flow region, the velocity can be described as:

$$U = a\,r\,;\; W = -2\,a\,z \qquad (16)$$

where **a** is the hydrodynamic constant. The hydrodynamic constant, **a**, has been correlated with the average nozzle exit velocity and the reactor geometry. Michaelidis [32] used:

$$a = \frac{w}{d^3 \cdot \rho} \cdot \left(3.1372 - 1.3533 \cdot \frac{L}{d} + 2.0109 \cdot \frac{L^2}{d^2} \right) \qquad (17)$$

where:

w = jet mass flow rate (g/s)
d = nozzle diameter (cm)
ρ = fluid density at nozzle exit (g/cm^3)
L = distance between end of nozzle and substrate (cm)

The pressure can be denoted by the Bernoulli equation:

$$p_o - p = -\frac{\rho}{2} \cdot \left(U^2 + W^2 \right) = -\frac{\rho \cdot a^2}{2} \cdot \left(r^2 + 4 \cdot z^2 \right) \qquad (18)$$

Thus, similar to inviscid flow theory, viscous flow uses the following hypothesis:

$$u = r\,f'(z)\;;\; w = -2\,f(z) \qquad (19)$$

$$p_o - p = -\,a^2\,(\,r^2 + F(z)\,) \qquad (20)$$

Note: prime (') represents partial derivative

While the continuity equation is satisfied exactly, the momentum equations become (with **f** and **F** as the main variables):

$$(f')^2 - 2\,f\,f'' = a^2 + \nu\,f''' \qquad (21)$$

$$2\,f\,f' + \nu\,f'' = 1/4\,a^2\,F' \qquad (22)$$

Boundary conditions:

$$z = 0;\ f = f' = 0 \qquad (23)$$

$$z = \infty;\ f' = a \qquad (24)$$

These equations could be solved if the constants **a** and ν were given, but a universal solution is more convenient. A similarity transformation frees the equations from constants **a** and ν. Choose:

$$\zeta = \left(\frac{a}{\nu}\right)^{\frac{1}{2}} \cdot z \qquad (25)$$

$$f(z) = (a \cdot \nu)^{\frac{1}{2}} \cdot \phi(\zeta) \qquad (26)$$

After much algebra, equation 21 simplifies as:

$$P''' + 2\,P\,P'' - (P')^2 + 1 = 0 \qquad (27)$$

Boundary conditions:

$$\zeta = 0;\ \phi = \phi' = 0 \qquad (28)$$

$$\zeta = \infty;\ \phi' = 1 \qquad (29)$$

The energy and species balance equations can also be reduced to one dimensional problems. Using equations 19, 25,and 26, substituting into 5, and simplifying, the energy equation becomes:

$$\frac{\partial^2 T}{\partial \zeta^2} + 2 \cdot \frac{\nu \cdot \rho \cdot C_p}{k} \cdot \phi \cdot \frac{\partial T}{\partial \zeta} = 0 \qquad (30)$$

Boundary conditions:

$$\zeta = 0;\ T = T_{wall} \qquad (31)$$

$$\zeta = \infty; T = T_{bulk} \qquad (32)$$

Likewise for the species balance equations, substituting equations 19, 25, and 26 into 6 results in:

$$\frac{\partial^2 x_i}{\partial \zeta^2} + \frac{2 \cdot \nu}{D} \cdot \phi \cdot \frac{\partial x_i}{\partial \zeta} - \sum_j a_{ij}^g \cdot N_i^g = 0 \qquad (33)$$

Boundary conditions:

$$\zeta = 0; D\left(\frac{a}{\nu}\right)^{\frac{1}{2}} \cdot \frac{\partial x_i}{\partial \zeta} = -\sum_j a_{ij}^s \cdot N_i^s \qquad (34)$$

$$\zeta = \infty; x_i = x_{io} \qquad (35)$$

To evaluate N^s_j, a chemical reaction mechanism must be developed. For surface reactions, a Hinshelwood-type rate expression is commonly used: (29, 31, 32)

$$N_i^s = \left(k_f \cdot \prod_{i=1} x_i^{a'_{ia}} - k_b \cdot \prod_{i=1} x_i^{a'_{ib}} \right) \cdot \beta_v \qquad (36)$$

$$\beta_v = \frac{1}{1 + \sum_{i=1} K_i^s \cdot x_i^{b'_i}} \qquad (37)$$

where:
k_f = forward rate constant
k_b = backward rate constant
a^s_i, b^s_i = reaction coefficients
B_v = fraction of active available sites on substrate
K^s_i = equilibrium constant for adsorption/desorption
When $B_v = 1$, $N^s_i = N_i$. In other words, expression 36 can be used to calculate the homogeneous rate expressions with $B_v = 1$.

Finally, these equations can be solved using an iterative finite difference numerical method. After each iteration, however, the physical properties must be recalculated because they vary with temperature and concentration. Theories which can be used to calculate the physical properties include: ideal gas law, Chapman- Enskog theory for viscosity(33) Chapman-Enskog theory for diffusion coefficients(33), thermal conductivity, and heat capacity(34). Also, if the kinetic parameters are not known, they must be determined experimentally. The reaction rates, N^s_i, can not be directly measured, but the growth rate can. An estimation involving the net

incorporation of each reaction product into the film can be used. [32]

$$q = V^{film} \cdot \sum_{i=1}^{n} \left(\sum_{j=1}^{s} n_i^{film} \cdot a_{ij}^{s} \cdot R_j^{s} \right) \qquad (38)$$

where:
q = growth rate (length/time)
V^{film} = molar volume of film (length^3/mol)
n_i^{film} = number of atoms in species i

Using film thickness data, the kinetic parameters are evaluated using a nonlinear least squares method (such as the Marquardt method [35]. With the results, any u-velocity, w-velocity, pressure, temperature, or concentration profile of the reactor can be attained. The variables that must be specified are surface and bulk temperatures, inlet gas composition, inlet mass flow rate, nozzle diameter, distance between substrate and nozzle, and physical constant data. In summary, this model is used by:

1. Obtaining experimental data for the growth rate of the film.
2. Hypothesize a reaction mechanism.
3. Determine kinetic parameters by using the experimental conditions, a non-linear least squares method, and the transport equations given above.
4. Change the mechanism until the best fit results.
5. Use the model to gain information about effects of changes to the reactor system and the reaction sequence.

Figure 1

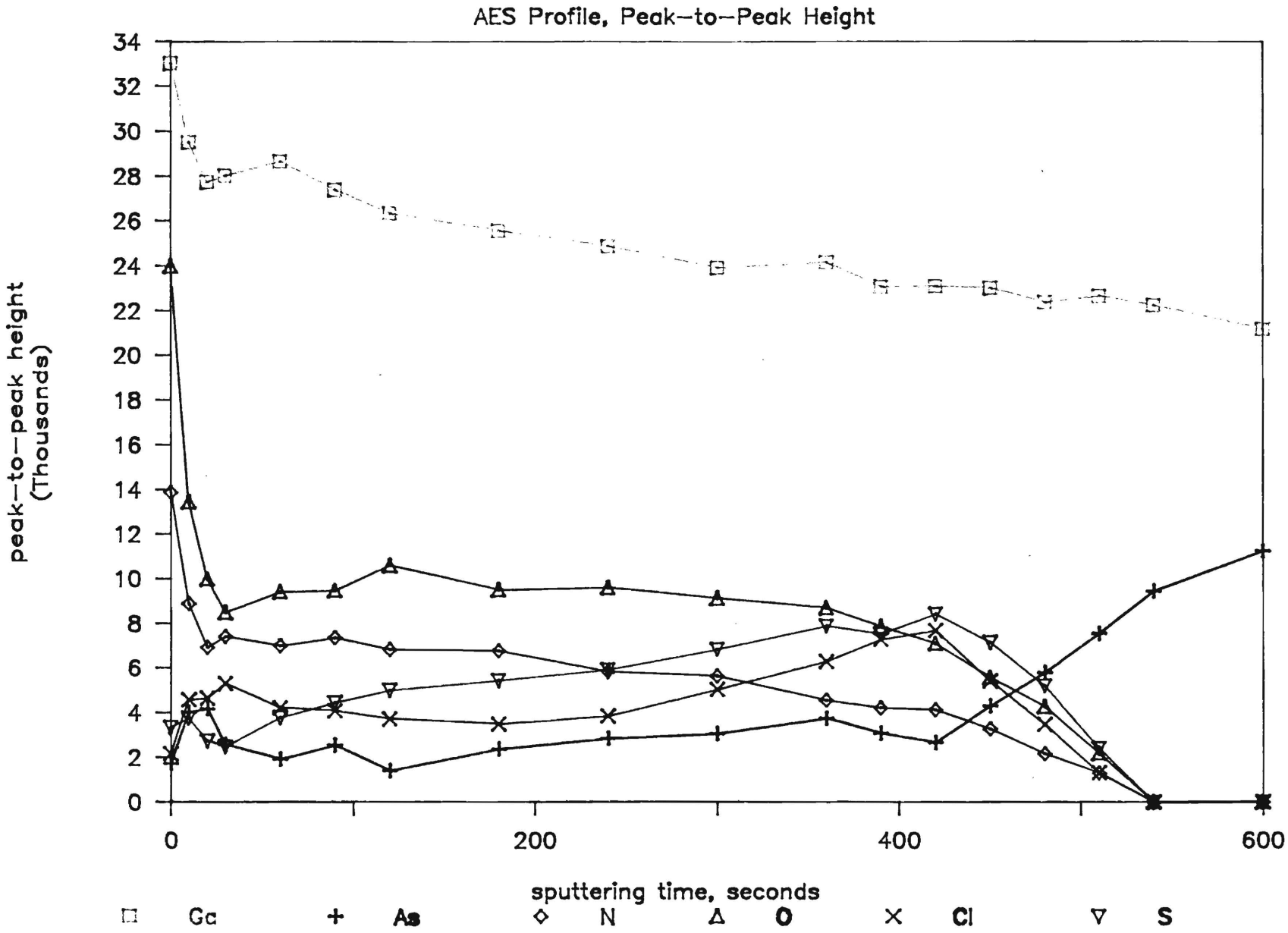
AES Profile, Peak–to–Peak Height
peak–to–peak height (Thousands)
34
32
30
28
26
24
22
20
18
16
14
12
10
8
6
4
2
0
0
200
400
600
sputtering time, seconds
Ga
As
N
O
Cl
S

Figure 2, Sensitivity Correction